University of Reading

Comparison of the self-assembly and cytocompatibility of conjugates of Fmoc (9-fluorenylmethoxycarbonyl) with hydrophobic, aromatic, or charged amino acids

Article

Published Version

Creative Commons: Attribution 4.0 (CC-BY)

Open Access

Castelletto, V., de Mello, L., da Silva, E. R. ORCID: https://orcid.org/0000-0001-5876-2276, Seitsonen, J. and Hamley, I. W. ORCID: https://orcid.org/0000-0002-4549-0926 (2024) Comparison of the self-assembly and cytocompatibility of conjugates of Fmoc (9-fluorenylmethoxycarbonyl) with hydrophobic, aromatic, or charged amino acids. Journal of Peptide Science. ISSN 1099-1387 doi: https://doi.org/10.1002/psc.3571 Available at https://centaur.reading.ac.uk/115291/

It is advisable to refer to the publisher's version if you intend to cite from the work. See Guidance on citing.

To link to this article DOI: http://dx.doi.org/10.1002/psc.3571

Publisher: European Peptide Society and John Wiley & Sons

All outputs in CentAUR are protected by Intellectual Property Rights law,

University of Reading

including copyright law. Copyright and IPR is retained by the creators or other copyright holders. Terms and conditions for use of this material are defined in the End User Agreement.

www.reading.ac.uk/centaur

CentAUR

Central Archive at the University of Reading

Reading's research outputs online

Check for updates

Received: 14 December 2023 | Revised: 24 January 2024 | Accepted: 25 January 2024

DOI: 10.1002/psc.3571

RESEARCH ARTICLE

Journal of PeptideScience WILEY

Comparison of the self-assembly and cytocompatibility of conjugates of Fmoc (9-fluorenylmethoxycarbonyl) with hydrophobic, aromatic, or charged amino acids

Valeria Castelletto[1] | Lucas de Mello[1,2] | Emerson Rodrigo da Silva[2] | Jani Seitsonen[3] | Ian W. Hamley[1]

[1]School of Chemistry, Food Biosciences and Pharmacy, University of Reading, Whiteknights, Reading, UK

[2]Departamento de Biofísica, Universidade Federal de São Paulo, São Paulo, Brazil

[3]Nanomicroscopy Center, Aalto University, Espoo, Finland

Correspondence
Ian W. Hamley, School of Chemistry, Food Biosciences and Pharmacy, University of Reading, Whiteknights, Reading RG6 6AD, UK.
Email: i.w.hamley@reading.ac.uk

Funding information
EPSRC, Grant/Award Number: EP/V053396/1

The self-assembly in aqueous solution of three Fmoc-amino acids with hydrophobic (aliphatic or aromatic, alanine or phenylalanine) or hydrophilic cationic residues (arginine) is compared. The critical aggregation concentrations were obtained using intrinsic fluorescence or fluorescence probe measurements, and conformation was probed using circular dichroism spectroscopy. Self-assembled nanostructures were imaged using cryo-transmission electron microscopy and small-angle X-ray scattering (SAXS). Fmoc-Ala is found to form remarkable structures comprising extended fibril-like objects nucleating from spherical cores. In contrast, Fmoc-Arg self-assembles into plate-like crystals. Fmoc-Phe forms extended structures, in a mixture of straight and twisted fibrils coexisting with nanotapes. Spontaneous flow alignment of solutions of Fmoc-Phe assemblies is observed by SAXS. The cytocompatibility of the three Fmoc-amino acids was also compared via MTT [3-(4,5-dimethylthiazol-2-yl)-2,5-diphenyltetrazolium bromide] mitochondrial activity assays. All three Fmoc-amino acids are cytocompatible with L929 fibroblasts at low concentration, and Fmoc-Arg shows cell viability up to comparatively high concentration (0.63 mM).

KEYWORDS
amino acids, cell culture, cytocompatibility, fibrils, Fmoc, self-assembly

1 | INTRODUCTION

Attachment of bulky terminal groups to peptides can drive self-assembly behavior, for example, fibril formation.[1–6] This self-assembly and diverse functionalities (bioactivity, biocatalytic activity, optoelectronic properties, etc.) of such N-terminal substituted peptides have recently been reviewed.[7] Bulky aromatic units such as Fmoc [9-fluorenylmethoxycarbonyl] undergo π-π stacking, which enhances self-assembly, that also depends on hydrophobic effects, hydrogen bonding, and electrostatic interactions between the peptide residues. Self-assembly leads to the possibility to produce hydrogels that may be used in the development of biomaterials for 3D cell culture. Fmoc-amino acids (Fmoc-aa's) (such as those shown in Scheme 1) were originally introduced in solid-phase synthesis in which the Fmoc group serves as a protecting group; however, over the last 20 years, many researchers have examined the self-assembly and properties of conjugates in which the Fmoc group is left attached to the peptide.

Several Fmoc-aa's can self-assemble into distinct nanostructures. Fmoc-Phe forms fibrillar hydrogels,[8,9] and Fmoc-Leu forms hydrogels when mixed with Fmoc-Lys.[10,11] Fluorescence spectra of Fmoc-Phe have been reported,[12] and the hydrogelation process has been monitored with fluorescent probes,[8,13] along with FTIR and NMR

This is an open access article under the terms of the Creative Commons Attribution License, which permits use, distribution and reproduction in any medium, provided the original work is properly cited.
© 2024 The Authors. *Journal of Peptide Science* published by European Peptide Society and John Wiley & Sons Ltd.

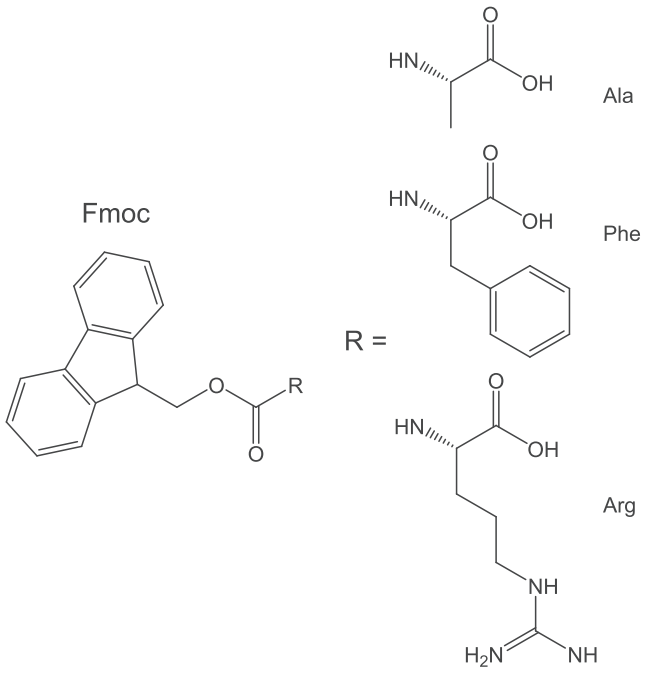

SCHEME 1 Schematic of Fmoc-amino acids studied.

analysis.[13] Fmoc-Phe can form hydrogels by acidification using the slow hydrolysis of glucono-δ-lactone.[14] The hydrogels have a fibrillar structure[9,14] and show slow-release properties of entrapped model dyes.[14] Later, hydrogelation was examined further for Fmoc-Phe along with that of other Fmoc-aa's Fmoc-Tyr, Fmoc-Trp, Fmoc-Met, Fmoc-Gly, and Fmoc-Ile.[15] The cases of Fmoc-Tyr and Fmoc-Phe crystals (plate- and needle-shaped, respectively) were observed to form in the gel phase, and this enabled crystal structures to be obtained for Fmoc-Tyr and Fmoc-Phe, and fiber diffraction patterns were also measured.[15] The properties of Fmoc-Phe gels and co-gels with other Fmoc amino acids have been reported, with demonstrated antimicrobial activity against Gram-positive bacteria.[16] Fmoc-Ala and Fmoc-His have been shown to undergo a self-assembly process starting from initial liquid–liquid phase separation of droplets, followed by fibril nucleation, over a timescale of hours.[17]

A number of Fmoc-aa's and Fmoc-dipeptides (and mixtures) have been shown to have good biocompatibility, and hydrogels have a suitable stiffness for cell culture applications. This has been the basis of commercial technology, for example, mixtures containing Fmoc-Ser, Fmoc-diphenylalanine (Fmoc-FF), and/or Fmoc-RGD, marketed by biogelx.[18–20] Here, the tripeptide RGD is a fibronectin-based integrin adhesion motif.[21–23] The development of these materials was based on earlier work, for example, Fmoc-FF can form fibril networks within hydrogel scaffolds for 3D cell culture, in mixtures with bioactive Fmoc-RGD.[24] Mixtures of Fmoc-FF with Fmoc-Lys, Fmoc-Asp, or Fmoc-Ser were also investigated for 2D and 3D culturing of several types of cell, and Fmoc-FF/Fmoc-Ser hydrogels were compatible with all three types of cell examined and can support 3D culture of chondrocytes.[25] Fmoc-peptides can be used to create hydrogels with other applications including wound healing[11] or for enzyme immobilization,[26] or slow release of encapsulated cargo (model dyes).[13]

Here, we investigate conditions for the self-assembly of three types of Fmoc-aa in aqueous solution. Conjugates containing one of three amino acids are examined: hydrophobic non-aromatic aliphatic L-alanine (A), hydrophobic aromatic L-phenylalanine (F), and cationic L-arginine (R) (Scheme 1). As mentioned above, the self-assembly of Fmoc-Phe has previously been examined under defined conditions (pH 6.6 for hydrogelation at 55°C[8] or 50 mM phosphate buffer within a very narrow pH range of 7.00 to 7.66[9]). During the preparation of this manuscript, we became aware of a report that discusses the self-assembly (in water or mixed water/THF) of Fmoc-Ala in comparison to Fmoc conjugates to Val, Leu, Ile, Pro, or Gly.[27] Among these, only Fmoc-Ala was found to form crystalline structures driven by Fmoc stacking. There do not appear to be studies on the bioactivity for the three Fmoc-aa's that are the focus of the present manuscript. This article complements our recent paper on the self-assembly and biocompatibility of Smoc-Ala, Smoc-Arg, and Smoc-Phe where Smoc denotes the water-soluble disulfonated Fmoc analogue 2,7-disulfo-9-fluorenylmethoxycarbonyl.[28] We do not directly compare the results due to the differences in solution conditions used to examine the two systems that arise from the significantly higher hydrophobicity of Fmoc.

Since these Fmoc-aa's are quite hydrophobic and do not show high solubility when dissolved in water at native pH, we first identify optimal conditions for aqueous solubility of the three conjugates by adjustment of pH and/or buffer. Then, having identified conditions for good aqueous solubility, molecular conformation is probed using circular dichroism and FTIR spectroscopy. Critical aggregation concentrations are determined from fluorescence probe assays. Self-assembly is investigated using both cryo-TEM imaging and small-angle X-ray scattering (SAXS). Cytocompatibility to L929 fibroblasts is assessed using MTT [3-(4,5-dimethylthiazol-2-yl)-2,5-diphenyltetrazolium bromide] assays, again observing conditions for solubility in the cell media used.

2 | EXPERIMENTAL

2.1 | Materials

Fmoc-L-Ala (Mw: 311.33 g/mol) and Fmoc-L-Phe (Mw: 387.43 g/mol) were purchased from NovaBiochem (Hohenbrunn, Germany) while Na-Fmoc-L-Arg (Mw: 396.45 g/mol) was obtained from ThermoFisher (UK). In the following, the samples are denoted Fmoc-Ala, Fmoc-Phe, and Fmoc-Arg.

2.2 | Sample preparation

Solutions were prepared by weighing controlled amounts of peptide and water. Solubility of the peptides was challenging due to the Fmoc

10991387, 0, Downloaded from https://onlinelibrary.wiley.com/doi/10.1002/psc.3571 by Test, Wiley Online Library on [08/03/2024]. See the Terms and Conditions (https://onlinelibrary.wiley.com/terms-and-conditions) on Wiley Online Library for rules of use; OA articles are governed by the applicable Creative Commons License

unit. Fmoc-Phe and Fmoc-Ala could be dissolved in basic conditions, while Fmoc-Arg was dissolved in acidic conditions; 1.5 wt% NaOH solution was titrated as necessary to obtain the desired basic solutions, while 0.5% acetic acid was used as a solvent for the acidic conditions. In this work, we dissolved up to 1 wt% Fmoc-Phe or Fmoc-Ala at pH 8 and 11, respectively. As discussed below, we also prepared a Fmoc-Phe gel (1 wt% Fmoc-Phe pH 9), previously studied by other groups,[9,14,16] only as a reference for the CD profile of the peptide solution at 1 wt% Fmoc-Phe at pH 8. We dissolved up to 0.3 wt% Fmoc-Arg in 0.5% acetic acid resulting in a solution with pH 3.

2.3 | UV–vis absorption

Spectra were recorded using a Varian Cary 300 Bio UV–vis spectrometer. Solutions were loaded in a 10-mm light path Quartz cell.

2.4 | Fluorescence spectroscopy

Experiments were carried out using a Varian Cary Eclipse spectrofluorometer. Solutions were loaded in a 10 mm light path quartz cell.

A series of dilutions were prepared to study the intrinsic fluorescence of the peptides as a function of the peptide concentration. The series of dilutions were prepared from three different mother solutions consisting of 0.3 wt% Fmoc-Phe pH 8, 0.3 wt% Fmoc-Ala pH 11, and 0.3 wt% Fmoc-Arg in 0.5% acetic acid pH 3. The solutions were excited at 265 nm, and the emission fluorescence was measured from 285 to 480 nm. The wavelength of excitation was chosen from the corresponding peak of absorptions measured in UV–vis experiments. A Thioflavin T (ThT) fluorescence assay, routinely used to pinpoint the presence of peptide fibers in solution,[29–31] was performed for Fmoc-Phe because it formed fibers in solution. For the experiments, a series of dilutions in 5.0×10^{-3} wt % ThT was prepared starting from a mother solution containing 0.3 wt% Fmoc-Phe in 5.0×10^{-3} wt % ThT, pH 8. The fluorescence of ThT in the dilution series was excited at 440 nm, and the emission spectrum was measured from 460 to 750 nm.

2.5 | Circular dichroism (CD) spectroscopy

CD spectra were recorded using a Chirascan spectropolarimeter (Applied Photophysics, Leatherhead, UK). Solutions were placed between parallel plates (0.1 or 0.01 mm path length). Spectra were measured with a 0.5 nm step, 0.5 nm bandwidth, and 1 s collection time per step. The CD signal from the water background was subtracted from the CD data of the sample solutions. CD signals were smoothed using the Chirascan Software for data analysis. The residue of the calculation was chosen to oscillate around the average, to avoid artifacts in the smoothed curve.

2.6 | Fourier-transform infrared (FTIR) spectroscopy

Spectra were recorded for D_2O solutions using a Thermo-Scientific Nicolet iS5 instrument equipped with a DTGS detector, with a Specac Pearl liquid cell with CaF_2 plates. The pH of Fmoc-Phe and Fmoc-Ala samples was fixed by titration of a 1 wt% NaOD solution. A total of 128 scans for each sample were recorded over the range of 900–4000 cm^{-1}.

2.7 | Cryogenic-TEM (Cryo-TEM)

Imaging was carried out using a field emission cryo-electron microscope (JEOL JEM-3200FSC), operating at 200 kV. Images were taken in bright field mode and using zero loss energy filtering (omega type) with a slit width of 20 eV. Micrographs were recorded using a Gatan Ultrascan 4000 CCD camera. The specimen temperature was maintained at −187°C during the imaging. Vitrified specimens were prepared using an automated FEI Vitrobot device using Quantifoil 3.5/1 holey carbon copper grids with a hole size of 3.5 µm. Just prior to use, grids were plasma cleaned using a Gatan Solarus 9500 plasma cleaner and then transferred into the environmental chamber of a FEI Vitrobot at room temperature and 100% humidity. Thereafter, 3 µL of sample solution was applied on the grid, and it was blotted twice for 5 s and then vitrified in a 1/1 mixture of liquid ethane and propane at temperature of −180°C. The grids with vitrified sample solution were maintained at liquid nitrogen temperature and then cryo-transferred to the microscope.

2.8 | Small-angle X-ray scattering (SAXS)

Synchrotron SAXS experiments on solutions were performed using a BioSAXS setup on BM29 at the ESRF (Grenoble, France).[32] A few microliters of samples were injected via an automated sample exchanger at a slow and very reproducible rate into a quartz capillary (1.8 nm internal diameter), in the X-ray beam. The quartz capillary was enclosed in a vacuum chamber, to avoid parasitic scattering. After the sample was injected in the capillary and reached the X-ray beam, the flow was stopped during the SAXS data acquisition. The q range was 0.005–0.48 $Å^{-1}$, with $\lambda = 1.03$ Å and a sample-detector distance of 2867 mm. The images were obtained using a Pilatus Pilatus3-2M detector. Data processing (background subtraction, radial averaging) was performed using dedicated beamline software ISPYB.

2.9 | MTT assays

L929 murine fibroblasts were maintained with DMEM medium supplemented with 10% of fetal bovine serum (FBS), 2 mM of GlutaMAX™, and penicillin–streptomycin. The cells were incubated at 37°C inside a cell incubator with a controlled atmosphere of 5% CO_2

10991387, 0, Downloaded from https://onlinelibrary.wiley.com/doi/10.1002/psc.3571 by Test, Wiley Online Library on [08/03/2024]. See the Terms and Conditions (https://onlinelibrary.wiley.com/terms-and-conditions) on Wiley Online Library for rules of use; OA articles are governed by the applicable Creative Commons License

inside a cell incubator. Twenty-four hours prior to the assay, L929 cells were detached with trypsin and transferred to 96-well plates at a density of 6×10^3 cells per well. Cells were then incubated with Fmoc-aa's dissolved in the medium at the concentrations of 0.1 to 2×10^{-4} wt% for 72 h inside the cell incubator. Images of the cells incubated with the Fmoc-aa's were obtained phase contrast microscopy. After the incubation, the wells were washed three times with PBS and incubated for 4 h at 37°C with a 100 µL of 0.05 wt% MTT dissolved in DMEM without phenol red. The resulting formazan crystals were dissolved by adding 100 µL of DMSO and incubating the plate at 37°C for 45 min, protected from the light with aluminum foil. Absorbance values were determined at 560 nm using an automatic plate reader. Cell survival was expressed as a percentage of viable cells in the presence of Fmoc-aa's, compared to control cells grown only in DMEM without any amino acids. The assay was made in triplicate and repeated three times. Statistical significance was tested using ANOVA for multiple comparisons with Bonferroni correction. All analyses were performed using Prism 7.

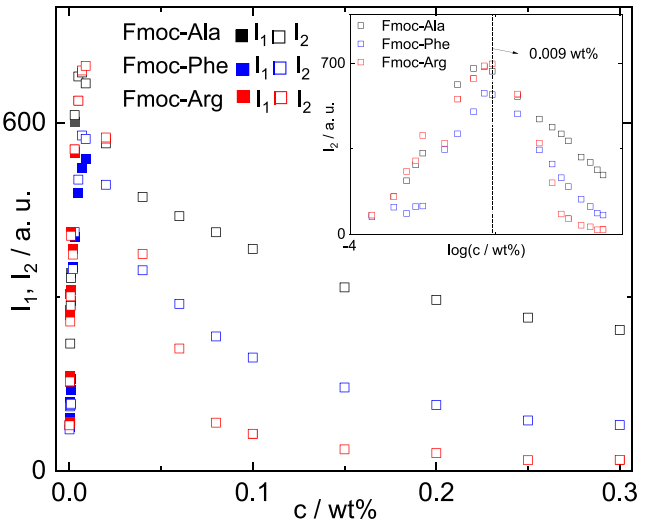

FIGURE 1 (a) Fmoc fluorescence emission intensities, I_1 and I_2, as a function of the concentration for Fmoc-Phe, Fmoc-Ala, and Fmoc-Arg.

3 | RESULTS

The three Fmoc-aa's studied show variable solubility in water, depending on pH or the presence of buffer (other groups have also explored the use of co-solvents such as THF). Good conditions for solubility with reasonable peptide concentration were found to be pH 11 aqueous solution for Fmoc-Ala, acetic acid (pH 3) for Fmoc-Arg, and near neutral aqueous solutions (pH 7–8) for Fmoc-Phe.

The presence of a potential critical aggregation concentration (CAC) for Fmoc-Ala, Fmoc-Arg, and Fmoc-Phe was examined using the intrinsic fluorescence of Fmoc following excitation at $\lambda_{ex} = 265$ nm, which is at the maximum observed in the measured UV–vis spectra (Figure S1), consistent with measurements for fluorene, Fmoc intrinsic, Fmoc-Phe derivatives, and Fmoc-peptides.[33,34] The intrinsic fluorescence of the peptides can also be studied by choosing $\lambda_{ex} = 285$ or 301 nm, with emission at $\lambda_{em} \sim 330$ nm.[35,36] The results of the intrinsic fluorescence CAC assays are shown in Figure 1 and show breaks at a CAC value $c = (0.009 \pm 0.001)$ wt% for all three samples. At this concentration, the initial maximum in the emission spectra at $\lambda = 305$ nm (I_1 Figure S2) has been replaced by a maximum due to aggregation (Fmoc excimer formation, I_2),[12] which is further red-shifted with increasing concentration, the maximum being located at $\lambda = 317$ nm, $\lambda = 319$ nm, and $\lambda = 325$ nm at the highest concentration studied (0.3 wt%) for Fmoc-Ala, Fmoc-Phe, and Fmoc-Arg, respectively (Figure S2). A large shift in the emission fluorescence spectral maximum upon aggregation was reported previously for Fmoc-Phe.[8,9]

Circular dichroism was used to probe chirality of superstructures and the presence of secondary structure. The CD data shown in Figure 2a–c reveal spectra comprising a negative minimum at 195 nm with weak peaks due to Fmoc at 214 nm and 228 nm[12] for Fmoc-Ala, consistent with a disordered and/or β-turn conformation.[37] However, the spectra for Fmoc-Arg in Figure 2b and Fmoc-Phe in Figure 2c contain features arising from the chiral packing of the fluorenyl group, and the spectrum for Fmoc-Phe (liquid at pH 7) shows features reported previously.[12] The peaks arising from the Fmoc group mask any strong typical signatures of peptide secondary structure, hindering the assignment of aggregation mode, although a soft gel of Fmoc-Phe at pH 9 shows a strong negative minimum at 230 nm, which may be a red-shifted minimum due to β-sheet structure.[38] Interesting differences are observed in the CD spectra for the samples at higher wavelengths above 250 nm, where contributions from secondary structure will have a minimal influence. In this region, the spectra are sensitive to the chiral ordering of aromatic moieties, that is, Fmoc (and Phe in the case of Fmoc-Phe). The CD spectrum for Fmoc-Ala in Figure 2a is featureless at higher wavelength, reflecting a lack of chiral order of Fmoc in this sample. However, the spectra for both Fmoc-Arg and Fmoc-Phe (Figure 2b,c) show notable features with a prominent peak at 305 nm along with smaller peaks at 295 nm and 285 nm. These can also be assigned to Fmoc (cf. the absorbance spectrum in Figure S1).[34] Peaks at these positions were also observed in the UV–vis absorption spectrum for Smoc-amino acids.[28] The spectra for Fmoc-Arg and Fmoc-Phe liquid (pH 8) are qualitatively similar in shape; however, a remarkable 'chiral inversion' for Fmoc-Phe is observed in the CD spectrum for the soft gel at pH 9. This reflects a change in the handedness of the twisted fibrils observed for Fmoc-Phe comparing liquid and soft gel and further information on this was provided by FTIR to be discussed shortly.

FTIR was used to complement CD to further elucidate the secondary structure of the peptides in solution. Results are displayed in Figures 2d–f. The spectrum for Fmoc-Ala in Figure 2d shows a peak at 1678 cm^{-1}, which can be assigned to β-turn structure[39,40] along with an amide II′ N-H/C-N deformation band at 1568 cm^{-1}.[40] The spectrum for Fmoc-Arg in Figure 2e shows a peak at 1614 cm^{-1} due to Arg guanidinium side chain deformations[41–46] and/or β-sheet

10991387, 0, Downloaded from https://onlinelibrary.wiley.com/doi/10.1002/psc.3571 by Test, Wiley Online Library on [08/03/2024]. See the Terms and Conditions (https://onlinelibrary.wiley.com/terms-and-conditions) on Wiley Online Library for rules of use; OA articles are governed by the applicable Creative Commons License

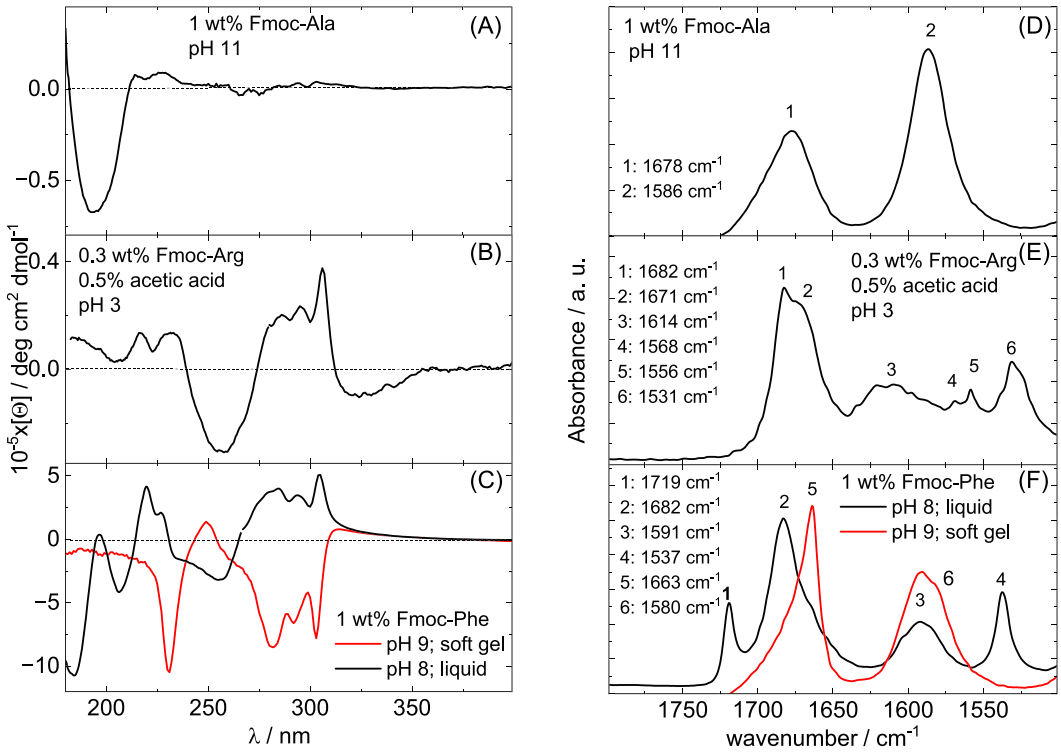

FIGURE 2 (a–c) CD and (d–f) FTIR spectra for 1 wt% Fmoc-Ala pH 11, Fmoc-Arg in 0.5% acetic acid, and Fmoc-Phe pH 8 (black line) and pH 9 (hydrogel, red line).

structure along with a peak at 1671 cm^{-1} due to β-sheet structure[39,40] and/or residual bound TFA counterions.[47–49] There are also amide II peaks, one of which at 1568 cm^{-1} can be assigned to an Arg guanidinium deformation mode.[41,42,44–46] Other modes may arise from Fmoc.[34] The spectrum for Fmoc-Phe contains a peak at 1682 cm^{-1} for the pH 8 liquid due to (antiparallel) β-sheet structure.[40,43,50] as well as a peak at 1719 cm^{-1} (for the solution, due to Fmoc carbamate[13]) along with amide II′ bands due to N-H/C-N and/or Fmoc deformations at lower wavelengths. There is a notable change in the spectrum in the pH 9 soft gel state, with a peak now at 1663 cm^{-1} signaling a transition from antiparallel β-sheet to a β-turn/parallel β-sheet structure, along with the loss of the C=O peak at 1719 cm^{-1}. This was reported previously for the FTIR spectrum of a lyophilized gel (prepared by thermal treatment from a phosphate buffer solution rather than pH, as here).[13] This was suggested to be either due to the involvement of the Fmoc carbonyl group in hydrogen bonding or the result of a different environment of Fmoc groups in the self-assembled structures in the gel.

For Fmoc-Phe, the potential presence of β-sheet structure led us to undertake a further CAC fluorescence assay using Thioflavin T (ThT) a dye sensitive to β-sheet 'amyloid' formation.[29–31,51] The intensity and position of the ThT fluorescence maxima are plotted in Figure 3 (the original fluorescence spectra are shown in Figure S3). The spectra show a large concentration-dependent shift from a broad maximum near 490 nm to a sharper peak at 550 nm at the highest concentration, with a significant discontinuity in the spectra between $c = 0.003$ wt% and $c = 0.005$ wt%, indicating a CAC = (0.004 ± 0.001) wt%. This is lower than the value obtained from the intrinsic Fmoc fluorescence (c = 0.009 wt%) and may indicate greater sensitivity of the ThT assay to aggregation and/or that initial β-sheet formation occurs at lower concentration than that at which Fmoc fluorescence is shifted due to aggregation.

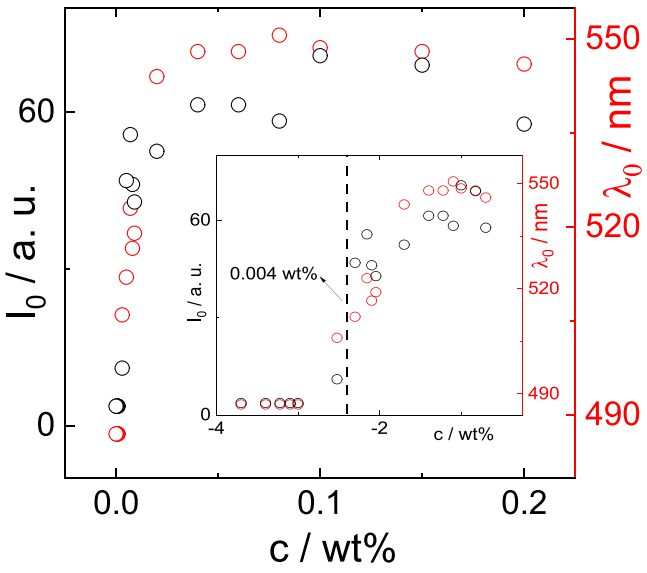

FIGURE 3 Peak intensity (I_0) and position (λ_0) measured from the ThT assay for Fmoc-Phe in solution at pH 8. The inset shows the results using a log-scale for concentration, to highlight the increase in I_0 and λ_0.

10991387, 0, Downloaded from https://onlinelibrary.wiley.com/doi/10.1002/psc.3571 by Test, Wiley Online Library on [08/03/2024]. See the Terms and Conditions (https://onlinelibrary.wiley.com/terms-and-conditions) on Wiley Online Library for rules of use; OA articles are governed by the applicable Creative Commons License

Having identified through fluorescence probe methods that all three Fmoc-aa's undergo aggregation above a CAC, we next examined the self-assembled structures above the CAC using both real-space cryo-TEM imaging and reciprocal-space SAXS. Figure 4 shows representative cryo-TEM images, and additional images are provided in Figure S4. Figure 4a indicates that Fmoc-Ala forms unusual structures with a diffuse spherical core from which one or more typically two extended fibril-like structures appear to protrude. These may arise from extended structures (fibrils or crystals) nucleating from a diffuse core. This has previously been reported for Fmoc-Ala on the basis of time-resolved studies which indicate initial liquid–liquid phase separation (in $AgNO_3$ solution) into droplets, followed by fibril nucleation.[17] The cryo-TEM images in Figure 4b show plate-like crystals for Fmoc-Arg. In contrast to these images for Fmoc-Ala and Fmoc-Arg showing crystallite-like structures, the images in Figure 4c for Fmoc-Phe contain extended self-assembled nanostructures, specifically a mixture of twisted and straight fibrils and wider nanotapes (as highlighted in parts i–iii). Thus, cryo-TEM suggests that both Fmoc-Ala and Fmoc-Arg form crystallites in aqueous solution, whereas Fmoc-Phe self-assembles into fibrils and nanotapes. The latter finding is consistent with prior reports on the formation of fibrillar hydrogels by Fmoc-Phe.[8,9,14]

To complement cryo-TEM, SAXS experiments were performed, these provide the form factors from self-assembled nanostructures formed in dilute solution.[52] The data are shown in Figure 5. The data for Fmoc-Ala have a low q slope in the power law $I(q) \sim q^{-\alpha}$ of $\alpha = 4$; this is consistent with Porod scattering from discrete objects such as the globular nuclei or crystallites shown in the cryo-TEM image in Figure 4a. The data for Fmoc-Arg show similar behavior with approximately the same low q scaling (due to the presence of isolated crystallites); however, there is (reproducibly) a Bragg peak observed at high q, corresponding to a d-spacing of 2.5 nm (Figure 5b). This is assigned to Fmoc-Arg packing in the plate-like crystals, possibly corresponding to one unit cell dimension. Powder XRD data were measured (data not shown), but a structure or unit cell could not be determined. In contrast to the other two samples, the SAXS data for Fmoc-Phe (Figure 5c) can be fitted to the form factor of a core–shell cylinder, consistent with a fibrillar structure. The fit parameters are listed in Table S1. The obtained core radius and shell thickness are consistent with a fibril bundle structure, the radius of 17.2 nm being significantly larger than the molecular dimensions. This is consistent with the presence of mixed aggregates in the cryo-TEM images (Figure 4c and Figure S4c). The SAXS data from this sample were anisotropic (Figure 5d), which reflects spontaneous alignment under flow during delivery to the capillary for the SAXS measurement. This is consistent with nematic phase formation by alignment of fibrils under flow (this could also be seen in some of the cryo-TEM images obtained).

Figure 6 shows data from MTT cytotoxicity assays for Fmoc-Ala, Fmoc-Arg, and Fmoc-Phe. The data show that at sufficiently low concentration, these conjugates are not cytotoxic. However, there is

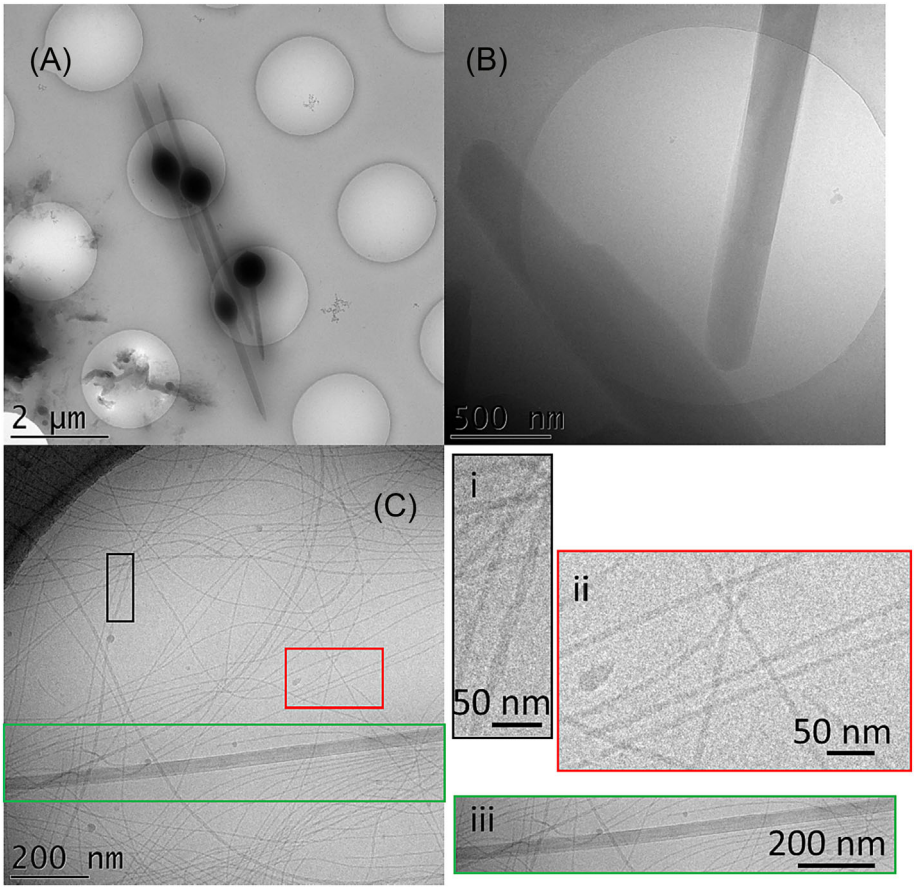

FIGURE 4 Representative cryo-TM images. (a) Fmoc-Ala, (b) Fmoc-Arg, and (c) Fmoc-Phe, including highlights/enlargements of selected nanostructures (i–iii).

10991387, 0, Downloaded from https://onlinelibrary.wiley.com/doi/10.1002/psc.3571 by Test, Wiley Online Library on [08/03/2024]. See the Terms and Conditions (https://onlinelibrary.wiley.com/terms-and-conditions) on Wiley Online Library for rules of use; OA articles are governed by the applicable Creative Commons License

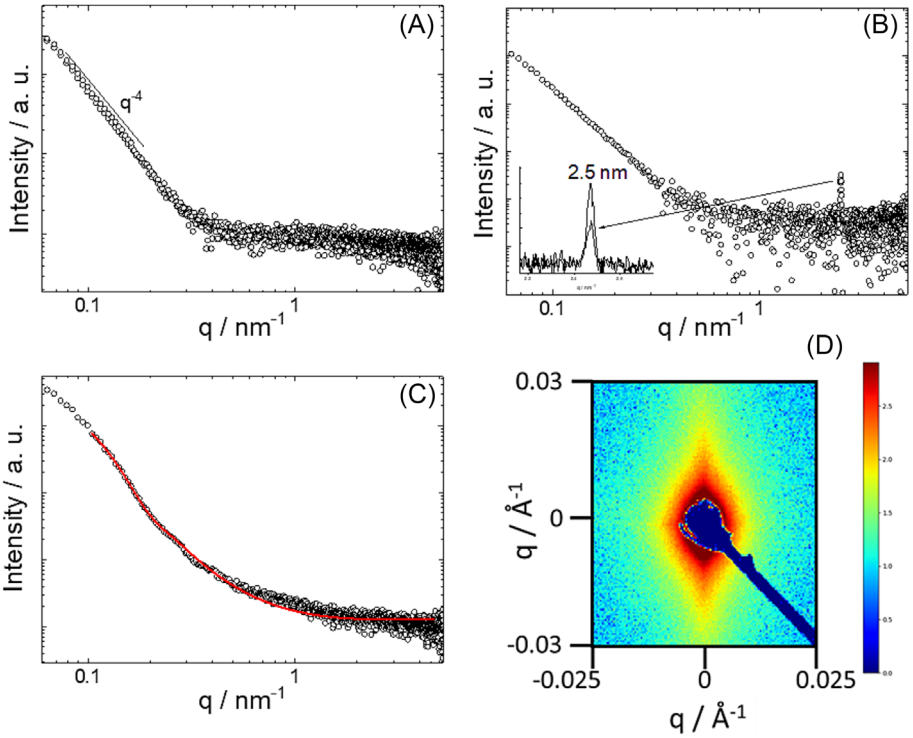

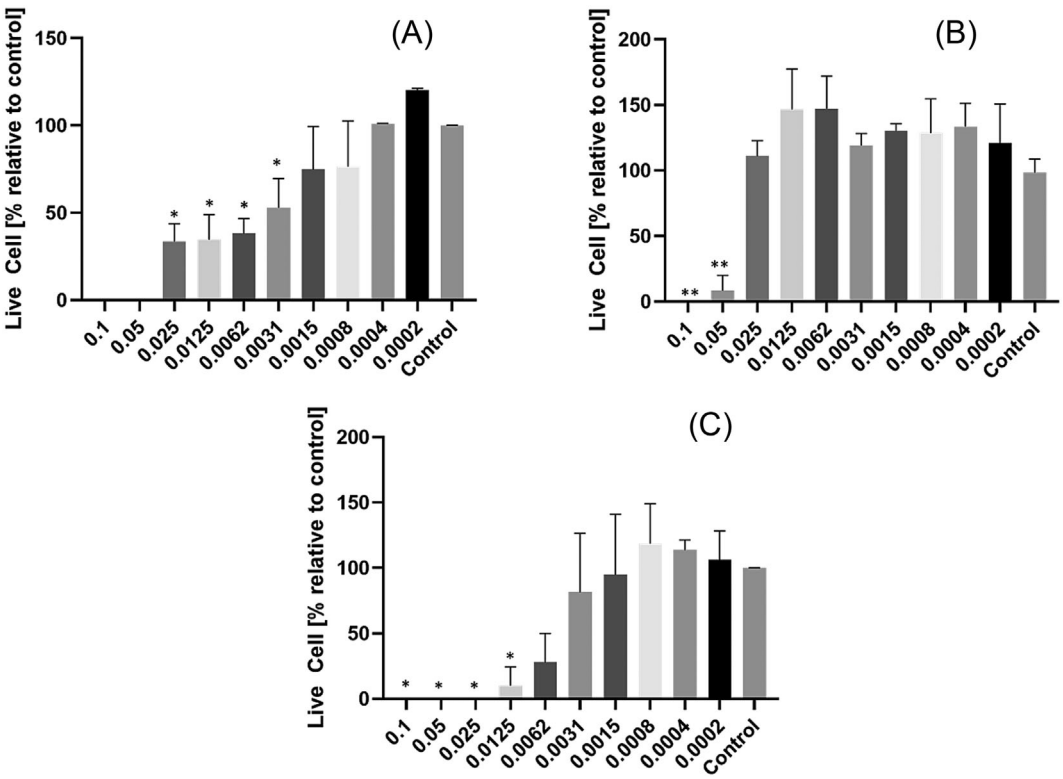

FIGURE 5 SAXS data for (a) 1 wt% Fmoc-Ala pH 11 and (b) 0.3 wt% Fmoc-Arg pH 3 in 0.5% acetic acid. The inset in (b) shows the distinctive peak in the SAXS curve, at 2.5 nm. (c) SAXS data and fit (red line), as described in the text, for 1 wt% Fmoc-Phe pH 8. (d) 2D SAXS pattern (logarithmic intensity scale) corresponding to 1D data in (c), showing the flow alignment of the peptide fibrils.

FIGURE 6 Cytocompatibility from MTT assays, after 72 h. (a) Fmoc-Ala, (b) Fmoc-Arg, and (c) Fmoc-Phe. Concentration of the Fmoc amino acids is expressed in wt%. * *p*-value below 0.05, ** *p*-value below 0.01, *** *p*-value below 0.001, all indicated by an ANOVA test with correction for multiple groups.

statistically significant reduced cytocompatibility when compared with the control for concentrations above 0.0031, 0.05, and 0.0125 wt% for Fmoc-Ala, Fmoc-Arg, and Fmoc-Phe, respectively. The data suggest that Fmoc-Arg is less cytotoxic than the other two, being fully cytocompatible below 0.025 wt% (0.65 mM). Fmoc-Phe seems to show an onset of cytotoxicity close to the CAC, that is, the

10991387, 0, Downloaded from https://onlinelibrary.wiley.com/doi/10.1002/psc.3571 by Test, Wiley Online Library on [08/03/2024]. See the Terms and Conditions (https://onlinelibrary.wiley.com/terms-and-conditions) on Wiley Online Library for rules of use; OA articles are governed by the applicable Creative Commons License

cytocompatibility shows a large reduction between 0.0031 and 0.0062 wt%, in the range of the CAC obtained from the ThT fluorescence assay, $c = 0.004$ wt% (Figure 4). Thus, for Fmoc-Phe, the cytotoxicity may be correlated to self-assembly. These findings are corroborated by the phase contrast images obtained with L929 cells incubated for 72 h with the Fmoc-aa's at concentrations of 0.1 wt% (Figures S5–S7), since the L929 cells presented an overall round morphology, related to fibroblasts under stress,[53,54] as opposed to the well spread fibroblasts exhibiting the expected morphology when incubated with an Fmoc-aa concentration 0.0625 wt%.

4 | DISCUSSION AND CONCLUSIONS

In this paper, the self-assembly and cytocompatibility of three Fmoc-aa's have been compared, selecting Fmoc-aa's containing hydrophobic, aliphatic Ala or hydrophilic Arg or hydrophobic, aromatic Fmoc-Phe. The apparent CAC values from Fmoc intrinsic fluorescence are the same for all three conjugates. Due to β-sheet formation (revealed by CD and the presence of fibrillar structures shown by cryo-TEM and SAXS), the CAC of Fmoc-Phe was also determined using the amyloid-sensitive dye Thioflavin T, and the CAC obtained was slightly lower than that from Fmoc intrinsic fluorescence. This was ascribed to higher sensitivity to aggregation or a slightly lower concentration for ThT-sensitive β-sheet formation than Fmoc fluorescence quenching due to aggregation. CD and FTIR were used to probe conformation and notable differences were observed; in particular, Fmoc-Ala shows a featureless CD spectrum and relatively few FTIR peaks, assigned to the presence of some β-turn structures above the CAC. In contrast, Fmoc-Arg and Fmoc-Phe show strong CD signals with signatures of chiral Fmoc order, with evidence for β-sheet ordering (signals at lower wavelength in the spectra) in the latter case, supported by FTIR (also possibly present to some extent for Fmoc-Arg). A notable chiral inversion is observed for Fmoc-Phe comparing solution and gels. The origin of this interesting effect is unclear in detail, although FTIR spectra (Figure 2f) indicate a change from antiparallel β-sheets in the pH 8 solution to parallel β-sheets at pH 9. This may cause a change in the handedness of the twist of the fibrils driven by changes of interactions (likely hydrogen bonding) involving Fmoc carbamate groups as revealed by FTIR (Figure 2f). This is clearly a subject for further research, and such effects could be elucidated by 2D-NMR, for example.

Cryo-TEM and SAXS reveal notable differences in the aggregation behavior of the three conjugates. Fmoc-Ala shows fibrillar crystal-like structures apparently nucleating from a spherical core, consistent with a recent report on this molecule in silver nitrate salt solution.[17] Those findings were interpreted in terms of the spherical domains resulting from liquid–liquid phase separation followed by amyloid fibril nucleation from the phase-separated droplets. Our results indicate that this can occur in basic (pH 11) solution without the presence of the salt. Fmoc-Arg forms plate-like crystals under the pH 3 conditions used to obtain sufficient aqueous solubility. The ordering of Fmoc-Arg will be driven by Fmoc-stacking interactions (as for Fmoc-Phe), but it should be noted that Arg-Arg interactions with hydrophobic π-π character are a possible contributor to the intermolecular interactions, as noted for Smoc-Arg.[28] Fmoc-Phe forms extended self-assembled fibril and nanotape structures under the basic pH 8 conditions employed. A coexistence of different straight, twisted fibril and nanotape structures is observed, i.e. there is notable polymorphism. The extended structures show spontaneous flow alignment as shown by anisotropic SAXS patterns.

The biocompatibility of the three Fmoc-aa's was compared for the first time. The MTT results obtained in this work showcase the cytocompatibility of the Fmoc-aa's in a range of concentrations. Fmoc-Ala and Fmoc-Phe were better tolerated at around 0.0031% and below (Figure 6b,c), while Fmoc-Arg was well tolerated below 0.05 wt% (Figure 6c). Overall, Fmoc-Arg was better tolerated at higher concentrations and with less variance than Fmoc-Ala and Fmoc-Phe. These results are a useful reference point for the future development of cell culture materials since mixtures of some of the studied Fmoc-amino acids (Fmoc-Phe) and related Fmoc-dipeptides have been commercially developed for such applications.

ACKNOWLEDGMENTS

This work was supported by EPSRC Fellowship grant (reference EP/V053396/1) to IWH. We thank Diamond for the award of SAXS beamtime on B21 (ref. SM29895-1) and Nikul Khunti for assistance and the ESRF for beamtime on BM29 (ref. MX-2513) and Dihia Moussaoui for help. We acknowledge the use of facilities in the Chemical Analysis Facility (CAF) at the University of Reading.

ORCID

Emerson Rodrigo da Silva https://orcid.org/0000-0001-5876-2276
Ian W. Hamley https://orcid.org/0000-0002-4549-0926

REFERENCES

1. Yang Z, Xu B. Supramolecular hydrogels based on biofunctional nanofibers of self-assembled small molecules. *J Mater Chem*. 2007;17(23):2385-2393. doi:10.1039/b702493b
2. Adams DJ. Dipeptide and tripeptide conjugates as low-molecular-weight hydrogelators. *Macromol Biosci*. 2011;11(2):160-173. doi:10.1002/mabi.201000316
3. Dasgupta A, Mondal JH, Das D. Peptide hydrogels. *RSC Adv*. 2013;3(24):9117-9149. doi:10.1039/c3ra40234g
4. Tomasini C, Castellucci N. Peptides and peptidomimetics that behave as low molecular weight gelators. *Chem Soc Rev*. 2013;42(1):156-172. doi:10.1039/c2cs35284b
5. Adler-Abramovich L, Gazit E. The physical properties of supramolecular peptide assemblies: from building block association to technological applications. *Chem Soc Rev*. 2014;43(20):6881-6893. doi:10.1039/c4cs00164h
6. Sheehan F, Sementa D, Jain A, et al. Peptide-based supramolecular systems chemistry. *Chem Rev*. 2021;121(22):13869-13914. doi:10.1021/acs.chemrev.1c00089
7. Hamley IW. Self-assembly, bioactivity and nanomaterials applications of peptide conjugates with bulky aromatic terminal groups. *ACS Appl Bio Mater*. 2023;6(2):384-409. doi:10.1021/acsabm.2c01041
8. Shi JF, Gao YA, Yang ZM, Xu B. Exceptionally small supramolecular hydrogelators based on aromatic-aromatic interactions. *Beilstein J Org Chem*. 2011;7:167-172. doi:10.3762/bjoc.7.23

10991387, 0, Downloaded from https://onlinelibrary.wiley.com/doi/10.1002/psc.3571 by Test, Wiley Online Library on [08/03/2024]. See the Terms and Conditions (https://onlinelibrary.wiley.com/terms-and-conditions) on Wiley Online Library for rules of use; OA articles are governed by the applicable Creative Commons License

9. Roy S, Banerjee A. Amino acid based smart hydrogel: formation, characterization and fluorescence properties of silver nanoclusters within the hydrogel matrix. *Soft Matter*. 2011;7(11):5300-5308. doi:10.1039/c1sm05034f
10. Yang ZM, Gu HW, Zhang Y, Wang L, Xu B. Small molecule hydrogels based on a class of antiinflammatory agents. *Chem Commun*. 2004;2:208-209. doi:10.1039/b310574a
11. Yang ZM, Xu KM, Wang L, et al. Self-assembly of small molecules affords multifunctional supramolecular hydrogels for topically treating simulated uranium wounds. *Chem Commun*. 2005;35(35):4414-4416. doi:10.1039/b507314f
12. Smith AM, Williams RJ, Tang C, et al. Fmoc-diphenylalanine self assembles to a hydrogel via a novel architecture based on π-π interlocked β-sheets. *Adv Mater*. 2008;20(1):37-41. doi:10.1002/adma.200701221
13. Singh V, Snigdha K, Singh C, Sinha N, Thakur AK. Understanding the self-assembly of Fmoc-phenylalanine to hydrogel formation. *Soft Matter*. 2015;11(26):5353-5364. doi:10.1039/c5sm00843c
14. Sutton S, Campbell NL, Cooper AI, Kirkland M, Frith WJ, Adams DJ. Controlled release from modified amino acid hydrogels governed by molecular size or network dynamics. *Langmuir*. 2009;25(17):10285-10291. doi:10.1021/la9011058
15. Draper ER, Morris KL, Little MA, et al. Hydrogels formed from Fmoc amino acids. *CrstEngComm*. 2015;17(42):8047-8057. doi:10.1039/c5ce00801h
16. Irwansyah I, Li YQ, Shi WX, et al. Gram-positive antimicrobial activity of amino acid-based hydrogels. *Adv Mater*. 2015;27(4):648-654. doi:10.1002/adma.201403339
17. Yuan CQ, Levin A, Chen W, et al. Nucleation and growth of amino acid and peptide supramolecular polymers through liquid-liquid phase separation. *Angew Chem Int Ed Engl*. 2019;58(50):18116-18123. doi:10.1002/anie.201911782
18. Alakpa EV, Jayawarna V, Lampel A, et al. Tunable supramolecular hydrogels for selection of lineage-guiding metabolites in stem cell cultures. *Chem*. 2016;1(2):298-319. doi:10.1016/j.chempr.2016.07.001
19. Harper MM, Connolly ML, Goldie L, et al. Biogelx: cell culture on self-assembling peptide gels. *Methods Mol Biol*. 2018;1777:283-303. doi:10.1007/978-1-4939-7811-3_18
20. Hedegaard CL, Mata A. Integrating self-assembly and biofabrication for the development of structures with enhanced complexity and hierarchical control. *Biofabrication*. 2020;12(3):032002. doi:10.1088/1758-5090/ab84cb
21. Ruoslahti E, Pierschbacher MD. Arg-Gly-Asp—a versatile cell recognition signal. *Cell*. 1986;44(4):517-518. doi:10.1016/0092-8674(86)90259-x
22. Ruoslahti E, Pierschbacher MD. New perspectives in cell-adhesion—RGD and integrins. *Science*. 1987;238(4826):491-497. doi:10.1126/science.2821619
23. Hamley IW. Small bioactive peptides for biomaterials design and therapeutics. *Chem Rev*. 2017;17(24):14015-14041. doi:10.1021/acs.chemrev.7b00522
24. Zhou M, Smith AM, Das AK, et al. Self-assembled peptide-based hydrogels as scaffolds for anchorage-dependent cells. *Biomaterials*. 2009;30(13):2523-2530. doi:10.1016/j.biomaterials.2009.01.010
25. Jayawarna V, Richardson SM, Hirst AR, et al. Introducing chemical functionality in Fmoc-peptide gels for cell culture. *Acta Biomater*. 2009;5(3):934-943. doi:10.1016/j.actbio.2009.01.006
26. Wang QG, Yang ZM, Wang L, Ma ML, Xu B. Molecular hydrogel-immobilized enzymes exhibit superactivity and high stability in organic solvents. *Chem Commun*. 2007;10(10):1032-1034. doi:10.1039/b615223f
27. Koshti B, Swanson HWA, Wilson B, et al. Solvent-controlled self-assembly of Fmoc protected aliphatic amino acids. *Phys Chem Chem Phys*. 2023;25(16):11522-11529. doi:10.1039/d2cp05938j
28. Castelletto V, de Mello L, da Silva ER, Seitsonen J, Hamley I. Self-assembly and cytocompatibility of amino acid conjugates containing a novel water soluble aromatic protecting group. *Biomacromolecules*. 2023;24(11):5403-5413. doi:10.1021/acs.biomac.3c00860
29. LeVine H. Thioflavine T interaction with synthetic Alzheimer's disease β-amyloid peptides: detection of amyloid aggregation in solution. *Protein Sci*. 1993;2(3):404-410. doi:10.1002/pro.5560020312
30. LeVine H. Quantification of β-sheet amyloid fibril structures with thioflavin T. In: Wetzel R, ed. *Methods in Enzymology*. Academic Press; 1999:274-284.
31. Hamley IW. Peptide fibrillisation. *Angew Chem Int Ed Engl*. 2007;46(43):8128-8147. doi:10.1002/anie.200700861
32. Pernot P, Round A, Barrett R, et al. Upgraded ESRF BM29 beamline for SAXS on macromolecules in solution. *J Synchrotron Radiat*. 2013;20(4):660-664. doi:10.1107/s0909049513010431
33. Ryan DM, Doran TM, Nilsson BL. Stabilizing self-assembled Fmoc-F_5-Phe hydrogels by co-assembly with PEG-functionalized monomers. *Chem Commun*. 2011;47(1):475-477. doi:10.1039/C0CC02217A
34. Zou Y, Razmkhah K, Chmel NP, Hamley IW, Rodger A. Spectroscopic signatures of an Fmoc-tetrapeptide, Fmoc and fluorene. *RSC Adv*. 2013;3(27):10854-10858. doi:10.1039/c3ra41979g
35. Reddy SMM, Shanmugam G, Duraipandy N, Kiran MS, Mandal AB. An additional fluorenylmethoxycarbonyl (Fmoc) moiety in di-Fmoc-functionalized L-lysine induces pH-controlled ambidextrous gelation with significant advantages. *Soft Matter*. 2015;11(41):8126-8140. doi:10.1039/c5sm01767j
36. Diaferia C, Rosa E, Gallo E, et al. Self-supporting hydrogels based on Fmoc-derivatized cationic hexapeptides for potential biomedical applications. *Biomedicine*. 2021;9(6):678. doi:10.3390/biomedicines9060678
37. Nordén B, Rodger A, Dafforn TR. *Linear Dichroism and Circular Dichroism:* A Textbook on Polarized-Light Spectroscopy. RSC; 2010.
38. Hamley IW, Nutt DR, Brown GD, Miravet JF, Escuder B, Rodríguez-Llansola F. Influence of the solvent on the self-assembly of a modified amyloid beta peptide fragment. II. NMR and computer simulation investigation. *J Phys Chem B*. 2010;114(2):940-951. doi:10.1021/jp906107p
39. Krimm S, Bandekar J. Vibrational spectroscopy and conformation of peptides, polypeptides and proteins. *Adv Protein Chem*. 1986;38:181-364. doi:10.1016/S0065-3233(08)60528-8
40. Stuart B. *Biological Applications of Infrared Spectroscopy*. Wiley; 1997.
41. Barth A. The infrared absorption of amino acid side chains. *Prog Biophys Mol Biol*. 2000;74(3-5):141-173. doi:10.1016/S0079-6107(00)00021-3
42. Barth A. Infrared spectroscopy of proteins. *Biochim Biophys Acta-Bioenerg*. 2007;1767(9):1073-1101. doi:10.1016/j.bbabio.2007.06.004
43. Castelletto V, Moulton CM, Cheng G, et al. Self-assembly of Fmoc-tetrapeptides based on the RGDS cell adhesion motif. *Soft Matter*. 2011;7(24):11405-11415. doi:10.1039/c1sm06550e
44. Castelletto V, Barnes RH, Karatsas K-A, et al. Restructuring of lipid membranes by an arginine-capped peptide bolaamphiphile. *Langmuir*. 2019;35(5):1302-1311. doi:10.1021/acs.langmuir.8b01014
45. Edwards-Gayle CJC, Castelletto V, Hamley IW, et al. Self-assembly, antimicrobial activity and membrane interactions of arginine-capped peptide bola-amphiphiles. *ACS Appl Bio Mater*. 2019;2(5):2208-2218. doi:10.1021/acsabm.9b00172
46. Edwards-Gayle CJC, Barrett G, Roy S, et al. Selective antibacterial activity and lipid membrane interactions of arginine-rich amphiphilic peptides. *ACS Appl Bio Mater*. 2020;3(2):1165-1175. doi:10.1021/acsabm.9b00894
47. Pelton JT, McLean LR. Spectroscopic methods for analysis of protein secondary structure. *Anal Biochem*. 2000;277(2):167-176. doi:10.1006/abio.1999.4320

10991387, 0, Downloaded from https://onlinelibrary.wiley.com/doi/10.1002/psc.3571 by Test, Wiley Online Library on [08/03/2024]. See the Terms and Conditions (https://onlinelibrary.wiley.com/terms-and-conditions) on Wiley Online Library for rules of use; OA articles are governed by the applicable Creative Commons License

48. Gaussier H, Morency H, Lavoie MC, Subirade M. Replacement of trifluoroacetic acid with HCl in the hydrophobic purification steps of pediocin PA-1: a structural effect. *Appl Environ Microbiol*. 2002;68(10):4803-4808. doi:10.1128/AEM.68.10.4803-4808.2002
49. Eker F, Griebenow K, Schweitzer-Stenner R. $A\beta_{1-28}$ fragment of the amyloid peptide predominantly adopts a polypropyline II conformation in acidic solution. *Biochemistry*. 2004;43(22):6893-6898. doi:10.1021/bi049542+
50. Jackson M, Mantsch HH. The use and misuse of FTIR spectroscopy in the determination of protein structure. *Crit Rev Biochem Mol Biol*. 1995;30(2):95-120. doi:10.3109/10409239509085140
51. Buell AK, Dobson CM, Knowles TPJ, Welland ME. Interactions between amyloidophilic dyes and their relevance to studies of amyloid inhibitors. *Biophys J*. 2010;99(10):3492-3497. doi:10.1016/j.bpj.2010.08.074
52. Hamley IW. *Small-Angle Scattering: Theory, Instrumentation, Data and Applications*. Wiley; 2021.
53. Rekha S, Anila EI. In vitro cytotoxicity studies of surface modified CaS nanoparticles on L929 cell lines using MTT assay. *Mater Lett*. 2019;236:637-639. doi:10.1016/j.matlet.2018.11.009
54. Sacco AM, Belviso I, Romano V, et al. Diversity of dermal fibroblasts as major determinant of variability in cell reprogramming. *J Cell Mol Med*. 2019;23(6):4256-4268. doi:10.1111/jcmm.14316

SUPPORTING INFORMATION

Additional supporting information can be found online in the Supporting Information section at the end of this article.

How to cite this article: Castelletto V, de Mello L, da Silva ER, Seitsonen J, Hamley IW. Comparison of the self-assembly and cytocompatibility of conjugates of Fmoc (9-fluorenylmethoxycarbonyl) with hydrophobic, aromatic, or charged amino acids. *J Pept Sci*. 2024;e3571. doi:10.1002/psc.3571

10991387, 0, Downloaded from https://onlinelibrary.wiley.com/doi/10.1002/psc.3571 by Test, Wiley Online Library on [08/03/2024]. See the Terms and Conditions (https://onlinelibrary.wiley.com/terms-and-conditions) on Wiley Online Library for rules of use; OA articles are governed by the applicable Creative Commons License